

Information Theory of Chemotactic Agents Using Both Spatial and Temporal Gradient Sensing

Julian Rode ^{1,2}, Maja Novak ^{2,3} and Benjamin M. Friedrich ^{1,2,*}

¹Physics of Life, TU Dresden, Dresden, Germany

²Center for Advancing Electronics Dresden, TU Dresden, Dresden, Germany

³University of Zagreb, Zagreb, Croatia

 (Received 11 March 2024; accepted 24 May 2024; published 18 June 2024; corrected 5 November 2024)

Biological cells and small organisms navigate in concentration fields of signaling molecules using two fundamental gradient-sensing strategies: spatial comparison of concentrations measured at different positions on their surface and temporal comparison of concentrations measured at different locations visited along their motion path. It is believed that size and speed dictate which gradient-sensing strategy cells choose, yet this has never been formally proven. Using information theory, we investigate the optimal gradient-sensing mechanism for an ideal chemotactic agent that combines spatial and temporal comparisons. We account for the physical limits of chemosensation: molecule counting noise at physiological concentrations and motility noise inevitable at the microscale. Our simulation data collapse onto an empirical power law that predicts an optimal weighting of information as a function of motility and sensing noise, demonstrating how spatial comparison becomes more beneficial for agents that are large, slow, and less persistent. This refines and quantifies the previous heuristic notion. Our idealized model assuming unlimited information processing capabilities serves as a benchmark for the chemotaxis of biological cells.

DOI: [10.1103/PRXLife.2.023012](https://doi.org/10.1103/PRXLife.2.023012)

I. INTRODUCTION

Biological cells employ two different gradient-sensing strategies for chemotaxis [1–3]: spatial comparison (SC), where a cell measures the external concentration of signaling molecules simultaneously at different positions on its surface, enabling it to directly estimate a spatial concentration gradient [4–8], and temporal comparison (TC), where a cell moves actively and determines whether the local concentration measured sequentially along its path increases or decreases in time [9–13]. Small bacteria such as *E. coli* employ TC, while larger and slower eukaryotic cells commonly employ SC. Gradient sensing allows these cells to move up concentration gradients. This chemotaxis enables bacteria to forage for food [9–11], social amoeba to aggregate [5–8], and immune cells to migrate to inflammation sites [4]. Sperm cells of marine invertebrates use a mixed strategy of temporal sampling along chiral paths to find the egg [14]. What is common to these examples is the paramount presence of noise.

In seminal work, Berg and Purcell investigated physical limits of chemosensation in light of sensing and motility noise [15]. Cells sense extracellular concentrations by detecting stochastic binding events of signaling molecules to specialized receptors on their surface, which, even if intracellular signaling were perfect, comprises inevitable molecule

counting noise. Thermal noise and active fluctuations during cell migration cause motility noise that randomizes cell orientation, rendering previous estimates of gradient direction uncertain [1,15]. The Berg-Purcell limit was later refined and fundamental sensing limits for either pure SC or TC were derived (see Refs. [16,17] for SC and Refs. [18–21] for TC). It was shown that biological cells operate at the information-theoretic limits of gradient sensing during chemotaxis if concentration gradients are shallow (see Refs. [6,7,22] for SC and Refs. [12,13,23,24] for TC).

However, the basic question, which of the two gradient-sensing strategies, SC or TC, provides more information for cells of a given size, is still open. As a first step towards an answer to this long-standing question, we consider here an ideal agent with unlimited information processing capabilities, building on recent advances in strategies involving information-theoretical characterization of optimal navigation [25–32]. While it would be naive to assume that single biological cells can perform the same information processing tasks, our ideal case serves as a baseline for the chemotaxis of biological cells [13] and can give hints on the evolutionary choice of gradient-sensing strategy.

We address both extremes of the exploitation-exploration trade-off, investigating greedy strategies that either maximize exploitation, i.e., use of existing information (maximum likelihood), or maximize exploration, i.e., acquisition of additional information (infotaxis). Infotaxis as pioneered by Vergassola *et al.* [25] harnesses the concept of information maximization from engineering [33] and provides an efficient and reliable heuristic for source-tracking problems [31]. It describes an idealized chemotactic agent that continuously updates a spatial likelihood map of putative target position based on noisy concentration measurements, moving at each

*Contact author: benjamin.m.friedrich@tu-dresden.de

Published by the American Physical Society under the terms of the [Creative Commons Attribution 4.0 International](https://creativecommons.org/licenses/by/4.0/) license. Further distribution of this work must maintain attribution to the author(s) and the published article's title, journal citation, and DOI.

time step in the direction that maximizes the expected information gain. A recent mathematical theory developed by Auconi extended the infotaxis model of Vergassola to spatially extended agents [34]. Here, we build on this theory, which we interpret as agents performing both SC and TC. Linearization of the originally nonlinear model enables efficient simulations. This allows us to dissect the optimal weighting of SC and TC in agents capable of both, akin to a nonlinear Kalman filter that optimally weights different noise-corrupted information sources [35], using as reference scenario static concentration fields established by a single source. We quantitatively show how SC becomes increasingly beneficial for agents of larger size that move slowly and with less directional persistence, suggesting why crawling eukaryotic cells use SC and swimming bacteria use TC.

II. SPATIAL AND TEMPORAL COMPARISON

Principally, chemotactic agents are characterized by their size a , speed v , and sensing rate J_0 at which chemoattractant molecules are detected, which may be assumed linear in concentration c as $J_0 = \lambda c$ [15], with rate constant λ that gauges sensing noise. Motility noise randomizes the direction of motion with the effective rotational diffusion coefficient D_{rot} .

An agent of finite size a can detect concentration differences across its diameter, with corresponding signal-to-noise ratio of gradient sensing by SC [7,16],

$$\text{SNR}^{\text{SC}} = \frac{a^2 t \lambda |\nabla c|^2}{c}, \quad (1)$$

where t denotes measurement time. Alternatively, for gradient sensing by TC, active motion enables agents to detect concentration changes at a rate $v \nabla c$ along their trajectory, with a signal-to-noise ratio that increases with the cubic power of measurement time t [21],

$$\text{SNR}^{\text{TC}} = \frac{v^2 t^3 \lambda |\nabla c|^2}{c}. \quad (2)$$

It has been proposed that effective measurement times are set by the rotational diffusion time $t \sim D_{\text{rot}}^{-1}$ on which swimming direction becomes randomized [1,36], yet recent works suggest more general power laws [37–39].

III. BAYESIAN CHEMOTAXIS COMBINING SPATIAL AND TEMPORAL COMPARISON

We present a minimal model of an ideal chemotactic agent combining SC and TC, to dissect the relative importance of SC for finding a target at the center of a radial concentration profile $c(\mathbf{x})$ of signaling molecules, assuming a baseline scenario of unlimited information processing capabilities. The agent is characterized by three fundamental parameters: size a , rate constant of molecule detection λ , and rotational diffusion coefficient D_{rot} (see Fig. 1) (all other parameters such as speed can be eliminated by rescaling space or time).

The agent continuously updates a likelihood map $p(\mathbf{x})$ of relative target position, based on the timing of molecule detection events *and* the position of detection on its circumference using Bayesian inference [see Eq. (A2) in the Appendix].

Different from Refs. [25,27,29–32], the agent uses a comoving egocentric map, which allows us to study motility noise. The expected change in information of this ideal chemotactic agent is the sum of two terms of information gain for SC and TC, respectively, and a loss term due to motility noise [see Eq. (A3)]. Active motion with velocity \mathbf{v} changes this expected information gain (to second order in the duration of the time step), again comprising an SC term (equal to the spatial gradient of a rate of information gain from SC) and a TC term (equal to a weighted gradient of the local rate of molecule detection) [see Eq. (A4)]. This analytical theory, developed in Ref. [34], is rewritten here in more compact form to highlight information gain from SC and TC. While the originally nonlinear theory was numerically challenging, a simple linearization proposed here speeds up simulations substantially.

Without loss of generality, we assume that agents move with constant speed $v = |\mathbf{v}|$. Changing v can be compensated by rescaling time, which rescales λ and D_{rot} ; likewise, changing concentration c is equivalent to changing λ .

The agent needs to choose its direction of motion in each time step. We tested two prototypical decision rules, which maximize either exploitation or exploration of information, respectively. In a maximum-likelihood (ML) strategy maximizing exploitation, the agent moves straight towards the global maximum of the current likelihood map $p(\mathbf{x}, t)$. Infotaxis provides a second possible navigation strategy, in which the agent chooses its velocity vector \mathbf{v} such that the expected change in information is maximized [25]. For our spatially extended agent, this is the case if \mathbf{v} maximizes Eq. (A4), which represents two possibly conflicting decision incentives, represented by the SC term and the TC term, respectively (see above). In the following, we study both strategies for different noise regimes and agent sizes.

IV. STEREOTYPIC NAVIGATION IN THE ABSENCE OF MOTILITY NOISE

We first simulated chemotactic agents without motility noise using either the maximum-likelihood strategy or infotaxis [see Fig. 2(a)]. Agents using infotaxis display stereotypic behavior and first move along a straight path whose direction is determined by initial conditions. After a characteristic turning event that defines a time t_{turn} , these agents home in on the target along approximately circular arcs. In contrast, agents using a maximum-likelihood strategy display more erratic motion before they move approximately ballistically to the target. Snapshots of likelihood maps shown as insets indicate that agents can swiftly estimate target distance, but less so target direction, as reflected by the initially annulus-shaped likelihood map. As agents accumulate directional information, these annulus-shaped distributions become crescent shaped. Occasionally, distributions become bimodal when agents move towards the center of the crescent (where likelihood is high), but do not sense the expected increase in molecule detection frequency, thus erasing likelihood there, which splits the crescent in two.

Bayesian updating is performed on the two-dimensional map of possible target positions, comprising information on both target distance and target direction. The estimated target

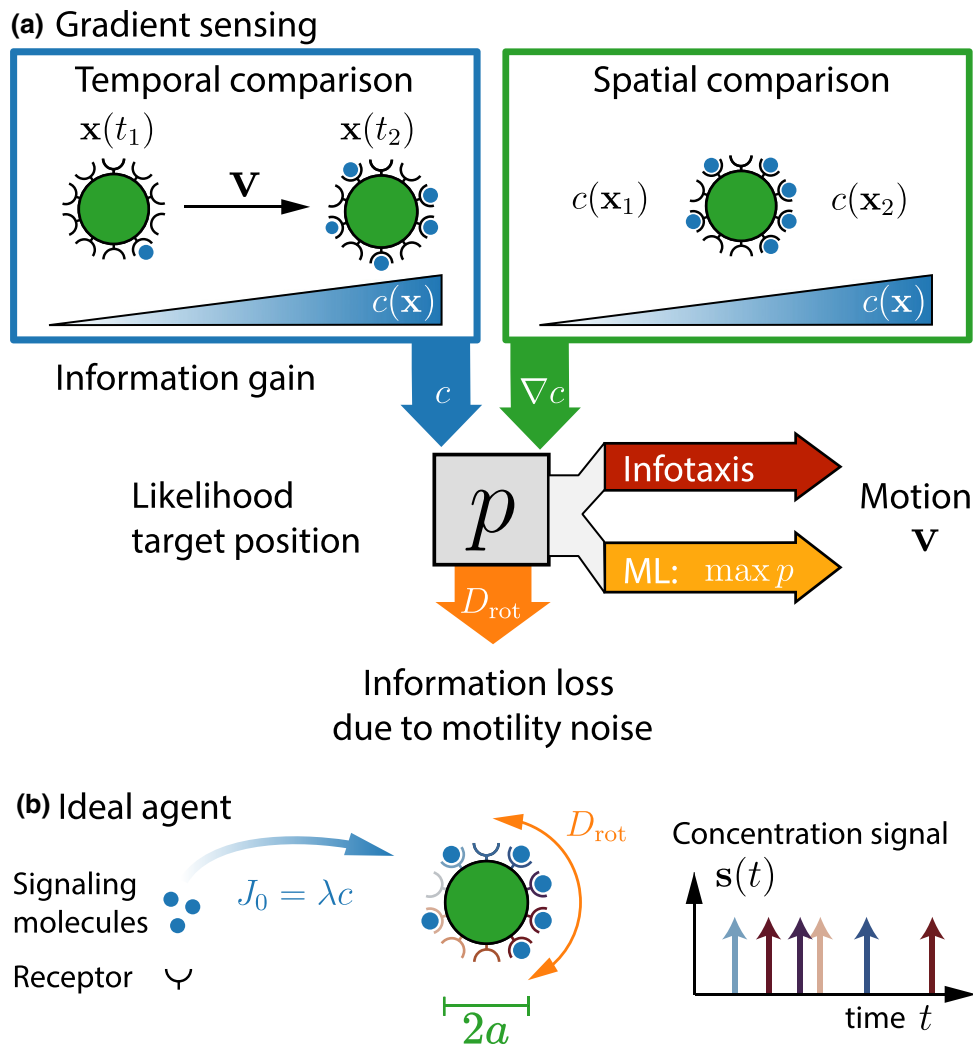


FIG. 1. Chemotactic navigation by temporal and spatial comparison. (a) Schematic of gradient sensing by temporal comparison, where chemotactic agents detect concentration differences along their motion path at different times (left), and spatial comparison, where agents detect concentration differences across their diameter (right). These strategies represent information sources, from which agents can infer a likelihood map $p(\mathbf{x})$ of target position \mathbf{x} . Agents make decisions on their next motion step with velocity \mathbf{v} based on this map using either the maximum-likelihood (ML) or infotaxis strategy. Motility noise randomizes motion direction and results in a continuous loss of information. (b) Model of an ideal agent that registers both time and position of signaling molecules binding at rate λc to receptors on its surface. The agent has size a ; motility noise is modeled by an effective rotational diffusion coefficient D_{rot} .

direction reflects cumulative gradient sensing by combined TC and SC. To monitor the gain in this directional information, we compute the negative Shannon entropy in bits $I_\varphi = -\int d\varphi p(\varphi) \log_2[2\pi p(\varphi)]$, where $p(\varphi)$ is the marginal distribution of the polar angle φ of relative target direction [see Fig. 2(b)]. For the uniform distribution $p(\varphi) = 1/(2\pi)$, $I_\varphi = 0$, reflecting the complete lack of directional information. When the agent gains information on target direction, and thus $p(\varphi)$ becomes more peaked, I_φ increases to become more positive. Indeed, the ensemble average of I_φ increases monotonically as a function of time, here normalized using the signal-to-noise ratio SNR^{TC} of TC [Eq. (2)]. The small spread of curves for infotaxis agents indicates that information gain before the first turning event is dominated by TC.

The characteristic turning events observed for infotaxis agents consistently occur when I_φ reaches the critical value of one bit [see Fig. 2(c); see also Fig. S1 in the Supplemental

Material (SM) [40] for more examples]. This is exactly the amount of directional information needed to judge whether the target lies in one half space or the other.

V. INFORMATION FLOW BALANCE WITH MOTILITY NOISE

Motility noise, modeled as effective rotational diffusion with diffusion coefficient D_{rot} , sets a finite persistence length $l_p = v/D_{\text{rot}}$ of agents (see Fig. 3), where $l_p = 1$ in Fig. 3(a) and $l_p = 0.2$ in Fig. 3(b). The randomization of swimming direction causes a continuous loss of information on putative target position. The result is a quasisteady state of information flow, where information gain due to chemosensation and information loss due to motility noise balance each other, reflected by a saturation of directional information $I_\varphi(t)$ at a maximal value I_φ^* [see Figs. 3(c) and 3(d)].

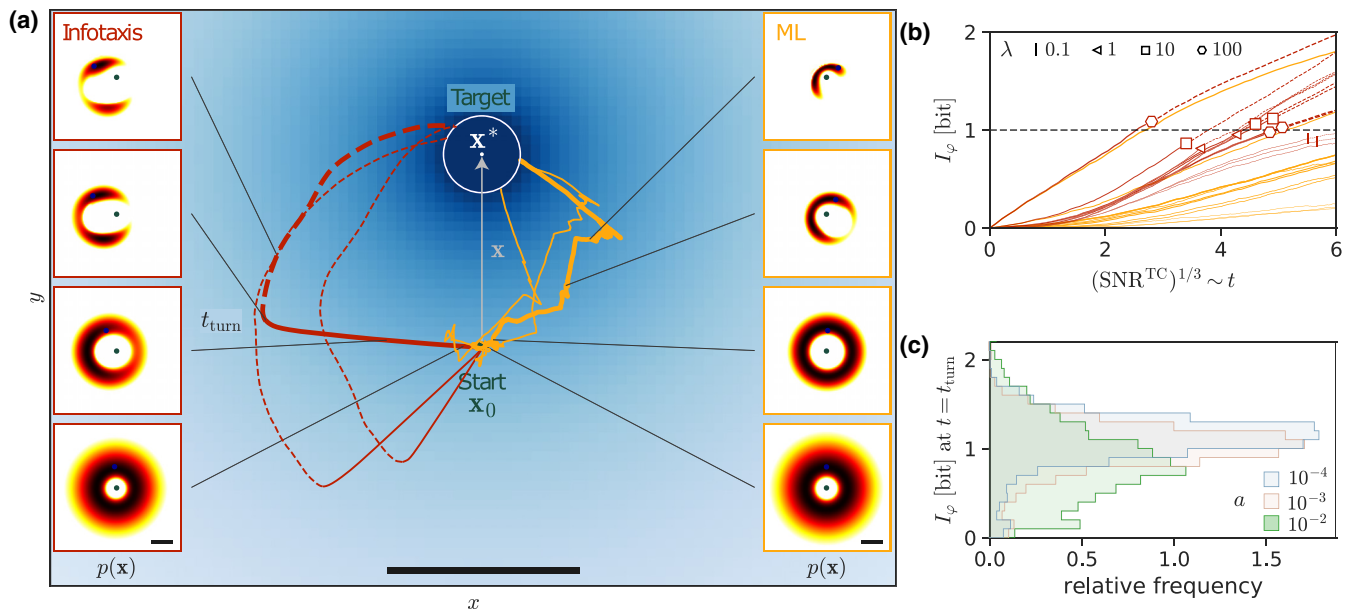


FIG. 2. Stereotypic motion without motility noise. (a) Typical trajectories of chemotactic agents (start point is green) navigating in a two-dimensional concentration field $c(x, y)$ of signaling molecules (blue) released by a target (dark blue). Agents use either a maximum-likelihood decision rule ML, (orange) or infotaxis maximizing the expected information gain (red). Insets depict likelihood maps $p(\mathbf{x})$ at selected times for one example trajectory each. For infotaxis, we distinguish a first straight section of the trajectories (solid) and a second section (dashed) after a turning point at time t_{turn} . The scale bar is 0.2 length units. (b) Directional information I_ϕ in target direction as a function of renormalized time expressed in terms of a signal-to-noise ratio SNR^{TC} of temporal comparison [Eq. (2)] for infotaxis (red) and ML (orange), for different values of the rate constant λ of molecule detection and agent size a (ensemble mean; symbols for infotaxis indicate the turning point with symbol shape indicating λ according to the legend and symbol size increasing with a). (c) Distribution of $I_\phi(t_{\text{turn}})$ at the first turning point for the case of infotaxis for different agent sizes (represented by line style, shown in the legend; data are pooled for different values of λ). The parameters are $D_{\text{rot}} = 0$ and (a) $a = 10^{-4}$ and $\lambda = 1$ and (b) and (c) $a = 10^{-4}$ – 10^{-2} and $\lambda = 1$ –100.

The mean angular information I_ϕ^* at this quasisteady state collapses onto a master curve $I_\phi^*(X)$ with a master parameter $X = \lambda^{0.28} D_{\text{rot}}^{-0.62} a^{0.10}$ that combines the rate constant λ of molecule detection, D_{rot} , and agent size a into an effective power law [see Figs. 3(e) and 3(f)]. Power-law exponents were determined by linear regression of the logarithm of I_ϕ^* (for infotaxis) as a function of the logarithms of the independent variables, which provides a robust collapse on a master curve even for this nonlinear functional relationship. The behavior for the maximum-likelihood strategy is remarkably similar. The exponents of the power law reflect the competition between information gain due to TC (characterized by λ) and SC (characterized by λa), and information loss (characterized by D_{rot}). A similar power law holds for the probability of agents to eventually find the target [see Fig. S2 in the SM [40], including Refs. [41–46]].

VI. RELATIVE IMPORTANCE OF SPATIAL COMPARISON

To gain further insight into the relative importance of temporal comparison versus spatial comparison for target finding, we computed their respective contributions to the directional information I_ϕ . While information decomposition remains challenging in general, we can make use of our analytical theory. For each information source, we computed the corresponding information gains dI_ϕ^{TC} and dI_ϕ^{SC} to I_ϕ using partial updates that involve only that term on the right-hand side of

the update equation (A2) that corresponds to this information source. By integrating over trajectories and averaging, we thus obtain the mean cumulated information gains I_ϕ^{TC} and I_ϕ^{SC} for TC and SC, respectively (conditioned on agents that found the target) (see the SM [40] for details). Figure 4(a) shows the relative fraction $\% \text{SC} = I_\phi^{\text{SC}} / (I_\phi^{\text{TC}} + I_\phi^{\text{SC}})$ of the information gain for SC as a function $\% \text{SC}(Y)$ of a second master parameter obeying a second empirical power law $Y = \lambda^{0.06} D_{\text{rot}}^{0.17} a^{0.77}$ obtained by a linear fit. All three exponents in this power law are positive. Agent size a has the largest exponent and is thus the presiding factor that determines the relative importance of spatial comparison. This is consistent with the strong dependence of the signal-to-noise ratio SNR^{SC} of SC on agent size a [see Eq. (1)]. An increase in motility noise (higher D_{rot}) likewise increases the contribution of SC. While rotational diffusion invalidates previously obtained directional information, irrespective of whether it was inferred from SC or TC, TC additionally requires a motion path as straight as possible to probe the concentration field and is thus more strongly affected by reduced directional persistence. An increase in sensing noise (lower λ) slightly reduces the contribution of SC. This indicates a higher vulnerability of SC to sensing noise, consistent with the notion that small concentration differences need to be compared across a relatively small distance in SC.

Because our theoretical analysis considers an ideal agent with unlimited information processing capabilities, it is not directly clear whether the behavior of biological cells is

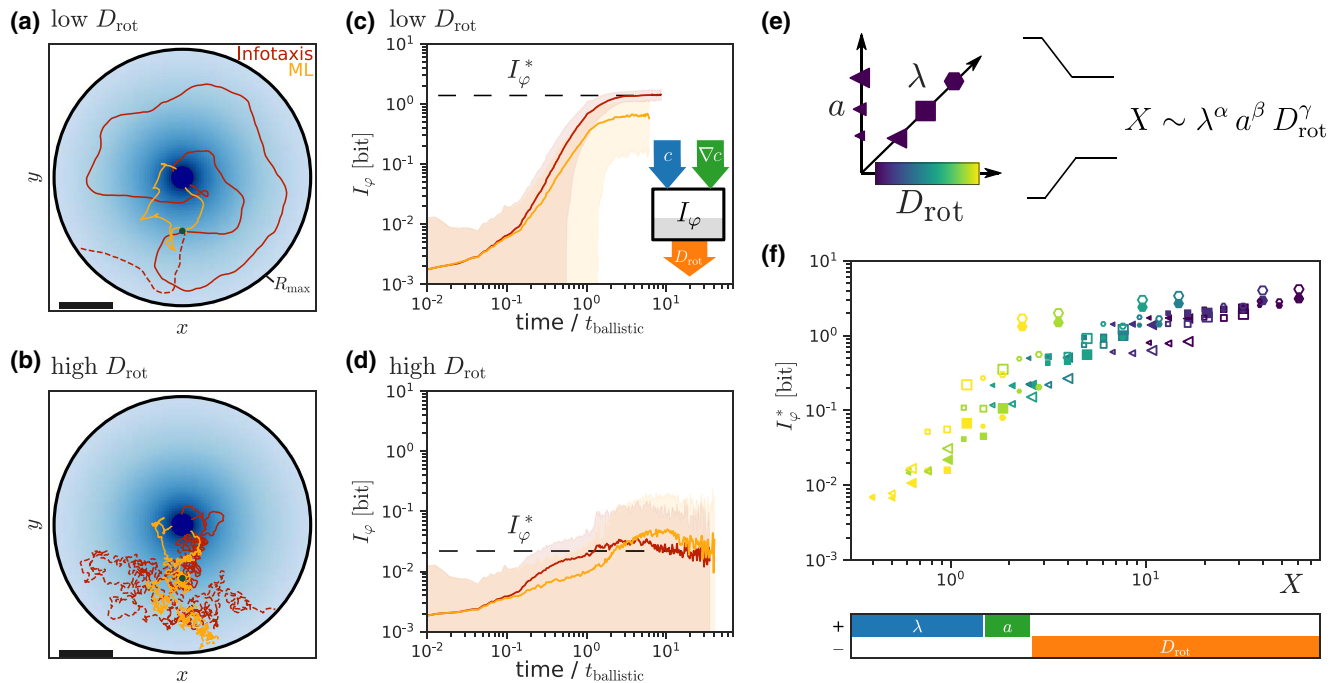


FIG. 3. Quasisteady state of information flow with motility noise. Typical trajectories of agents subject to motility noise are shown using either a maximum-likelihood strategy (orange) or infotaxis (red) with (a) low D_{rot} ($l_p = 1$) or (b) high D_{rot} ($l_p = 0.2$). Dashed trajectories failed to find the target, but reached the absorbing boundary (black) at R_{max} before. The scale bar is 0.2 length units. Plots of directional information I_φ as a function of normalized time $t/t_{\text{ballistic}}$ with $t_{\text{ballistic}} = R_{\text{target}}/v$ for cases of (c) low motility noise and (d) high motility noise reveal a quasisteady state of directional information with saturating directional information I_φ^* (orange shows the maximum-likelihood strategy and red infotaxis; ensemble mean \pm s.d.). The inset in (c) sketches information flow determining I_φ , with information gained by TC (blue) and SC (green) and lost due to motility noise (orange). (e) The three fundamental model parameters λ , D_{rot} , and a can be combined into a single empirical power law $X = \lambda^\alpha a^\beta D_{\text{rot}}^\gamma$ for any simulated quantity such as I_φ^* to test if that quantity collapses on a master curve as function of this single effective parameter X (with exponents determined by a linear fit of logarithms). (f) Quasisteady states of directional information collapse on a master curve $I_\varphi^* = I_\varphi^*(X)$ with the effective master parameter X that obeys an empirical power law $X = \lambda^{0.28} D_{\text{rot}}^{-0.62} a^{0.10}$ [the maximum-likelihood strategy is shown by open symbols and infotaxis by closed symbols; agent parameters are encoded according to the coordinate system in (e)]. Power-law exponents were determined for infotaxis agents by a multivariate fit and are visualized below the figure. The parameters (unless stated otherwise) are (a) and (c) $a = 0.01$, $\lambda = 1$, and $D_{\text{rot}} = 0.01$; (b) and (d) the same as in (a) but with $D_{\text{rot}} = 0.5$; and (e) and (f) $a = 10^{-4} - 10^{-2}$, $\lambda = 1 - 100$, and $D_{\text{rot}} = 5 \times 10^{-3} - 1$.

dictated by similar laws. Therefore, we reanalyzed data from 252 different cell types corresponding to four groups (prokaryotes, ciliates, flagellates, and cells with amoeboid motility) as reviewed in Ref. [2], as well as two unusual bacteria described in Refs. [47,48]. Figure 4(b) shows for each cell type the value of the power law derived in Fig. 4(a) for the ideal agent. Prokaryotes commonly perform gradient sensing by TC (with exceptions discussed below). Ciliates and flagellates employ a mixed strategy, known as helical klinotaxis, combining aspects of TC and SC, also reviewed below. Cells with amoeboid motility use chemotaxis by SC [5–7].

Spatial comparison was recently demonstrated for pili-based twitching chemotaxis of the bacterium *Pseudomonas aeruginosa* [47], marked by a plus in Fig. 4(b). A bacterium described in [48] and marked by a cross in Fig. 4(b) displays chemotaxis by SC at very high oxygen concentrations, corresponding to a high effective value of λ . Other bacteria that seem to deviate from the rule [open circles in Fig. 4(b)] likewise display unusual types of motility, such as pili-based motility or actin polymerization, or perform phototaxis instead of chemotaxis [2]. Figure 4(b) thus demonstrates that different cells employ temporal or spatial comparison exactly

when our idealized theory indicates a higher relative importance of one versus the other.

For the above comparison, agent sizes and speeds as reported in [2,47,48] were converted to values of the parameters λ , D_{rot} , and a , using a conservative estimate for D_{rot} that assumes rotational diffusion is set by thermal fluctuations, hence $D_{\text{rot}} \sim a^{-3}$ [49], while the diffusive flux of signaling molecules to the agent scales linearly with its size $\lambda \sim a$ [15]. With these assumptions and a rescaling of time to account for different speeds of cells, we can remap parameters and restate the empirical power law from Fig. 4(a) in terms of the directly measurable parameters cell size a (measured in microns) and speed v (measured in microns per second) [see Fig. 4(b), bottom, and the equivalent representation in Fig. 4(c)]. Explicitly, we used the initial target distance R_{target} as a typical length scale and $t_{\text{ballistic}} = R_{\text{target}}/v$ as typical timescale to write the power law from Fig. 4(a) in dimensionless form, for %SC(Y),

$$\begin{aligned}
 Y &\sim (\lambda c t_{\text{ballistic}})^{0.06} (D_{\text{rot}} t_{\text{ballistic}})^{0.17} (a/R_{\text{target}})^{0.77} \\
 &\sim \frac{a \text{ [\mu m]}^{0.32}}{v \text{ [\mu m/s]}^{0.23}}.
 \end{aligned} \tag{3}$$

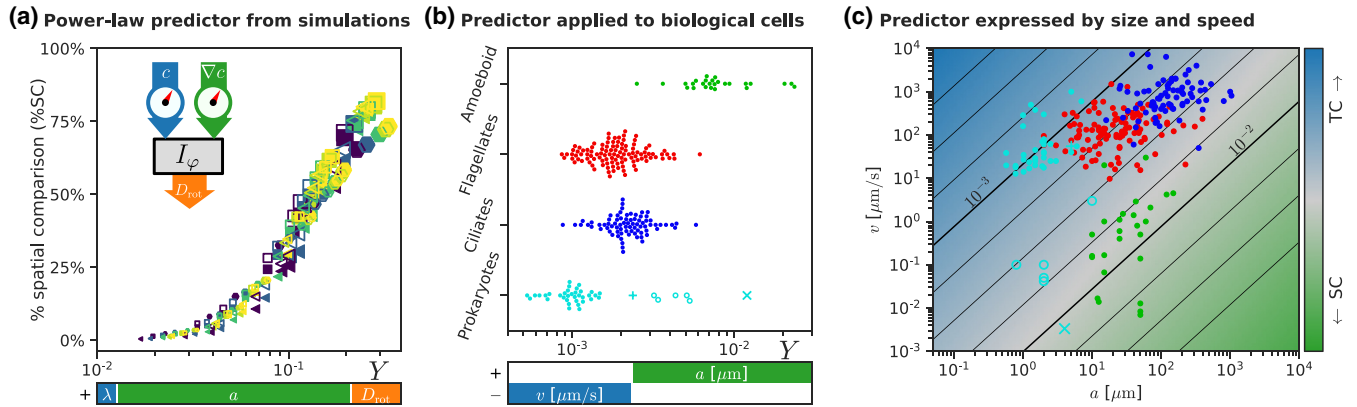


FIG. 4. Information decomposition reveals relative importance of spatial comparison. (a) The relative importance of spatial comparison %SC for target finding, computed by metering information flow, collapses on a master-curve %SC(Y) as a function of an effective master parameter Y that obeys an empirical power law $Y = \lambda^{0.06} D_{\text{rot}}^{0.17} a^{0.77}$, which combines all model parameters (the maximum-likelihood strategy is shown by open symbols and infotaxis by closed symbols; agent parameters are encoded according to the inset in Fig. 3). Specifically, we computed the cumulated gain in directional information using partial update steps corresponding to TC and SC according to Eq. (A2), respectively (see the text for details). Power-law exponents for Y were determined for infotaxis agents by a multivariate fit and are visualized below the figure. (b) Values of the predictor Y estimated for biological cells performing chemotaxis with data taken from [2], using the power law from (a) and making the conservative assumption that rotational diffusion is set by thermal fluctuations. The color code represents different navigation strategies: cyan, bacteria which mostly perform gradient sensing by temporal comparison (dots) and likely exceptions (other symbols, explained in the text); blue and red, ciliates and flagellates performing helical klinotaxis representing a mixed strategy; and green, eukaryotic cells with amoeboid motility performing chemotaxis by spatial comparison. The power law can be equivalently expressed as $a^{0.32}/v^{0.23}$ in terms of directly measurable parameters size a and speed v , using an assumption on the diffusion coefficient (see the SM [40]). (c) Data from [2] replotted in a - v parameter space, together with the empirical power law for the relative importance of spatial comparison, plotted using the same color code as in (a). The parameters are $a = 10^{-3} - (2 \times 10^{-2})$, $\lambda = 1 - 100$, $D_{\text{rot}} = 0.1 - 1$. In (b) and (c) the reference concentration $c = 1$ nM.

In the second line, we used the scaling of D_{rot} and λ as a function of the directly measurable quantities of size a and speed v (see the SM [40] for details).

By Eq. (3), additional factors can affect the relative importance of SC. The example of a bacterium using SC described in [48] from above is characterized by a 5000-fold increased value of λc relative to the reference value used otherwise. Accounting for this high value of λc and thus reduced sensing noise reflected in our predictor Y separates this unusual bacterium from other prokaryotes that perform TC. If only size a and speed v are considered as in Fig. 4(c), this is not possible.

Ciliates and flagellates shown in Figs. 4(b) and 4(c) employ a navigation strategy known as helical klinotaxis [2, 14, 50]. As in TC with a single effective sensor, these cells sample a scalar signal along their swimming path. However, swimming paths are helical, so in the course of a single helical turn, this sensor will have probed all directions, just like agents performing SC, thus enabling directed steering. Equation (1) could be extended to helical klinotaxis if instead of a the radius R of helical swimming paths is used. Helical klinotaxis is most efficient in three space dimensions and only possible if the persistence time D_{rot}^{-1} exceeds the period $T \sim R/v$ of helical swimming [2, 3].

In conclusion, our information-theoretic analysis explains the previous heuristic observation that large and slow cells commonly employ spatial comparison for gradient sensing, while small and comparatively fast cells use temporal comparison instead [1, 2, 51].

VII. A PHOTOTACTIC ROBOT

For demonstrative purposes and as a proof of principle that bioinspired Bayesian chemotaxis combining TC and SC may be applied in autonomous search robots (instead of using only TC [52–54]), we built a phototactic robot. Figure 5(a) shows our mecanum-wheeled toy robot capable of motion in all directions, which we equipped with a circular array of four light sensors connected to a control unit (see the SM [40] for details). Imperfections of the robot drive cause small deviations between control signal and actual movement, which we characterize by an effective rotational diffusion coefficient D_{rot} (see Fig. S12 in the SM [40]). As proxy for a scalar field corrupted by shot noise, the robot navigates in response to a fluctuating pixel pattern projected on the floor, where the flashing probability of each pixel is proportional to $\lambda c(x, y)$. The robot uses Bayesian inference as in simulations, but neglects its own motility noise as if $D_{\text{rot}} = 0$.

Camera-based tracking yields robot tracks that strongly resemble those in simulations [see Fig. 5(b)]. Changing the size of the sensory array provides a simple means to probe different effective sensing length scales a . The relative importance of spatial comparison in the corresponding robot experiments for different a [computed analogously to Fig. 4(b)] agrees well with simulation results [see Fig. 5(c)]. This demonstrates the feasibility of the approach, despite the complexities of a real robot with actuator noise, which are only partly captured by simulations.

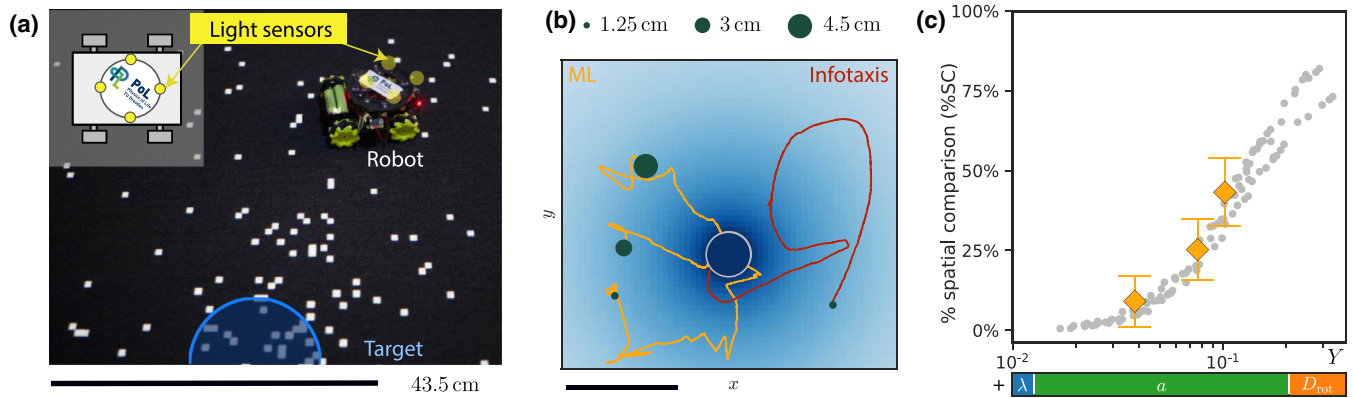


FIG. 5. Phototactic robot combining spatial and temporal comparisons. (a) Search robot equipped with an array of four light sensors exposed to a fluctuating pixel pattern projected on the floor. Robots navigate in response to this light stimulus using the same algorithm as ideal agents to find the center of a radial gradient of stochastically flashing pixels. (b) Typical tracks of robots using either maximum-likelihood decision strategy (orange) or infotaxis (red) with different sensor array sizes (green dots mark start positions; tracks are rotated for visual clarity). (c) The relative importance of spatial comparison (%SC) for target finding in experiments with ML robots with different sensor array sizes (orange, mean \pm s.d., $n = 22, 10, 14$) matches simulation data for simulated agents from Fig. 4(a) (gray dots), using a measured estimate $D_{\text{rot}} = 0.004$ (see the SM [40] for details). The scale bars in (a) and (b) are 43.5 cm (which maps to 0.2 length units).

VIII. DISCUSSION

We used information theory to compare two fundamental gradient-sensing strategies for chemotaxis, spatial comparison (SC) and temporal comparison (TC), by quantifying their relative importance in an ideal agent that combines both. Specifically, a minimal model of an chemotaxis agent with unlimited information processing capabilities allowed us quantify “chemotaxis in bits” in a baseline scenario. An analytical theory allows explicit information decomposition and thus to dissect the relative importance of SC versus TC, which collapses on a master curve. The corresponding power law (3) reflects the expected competition between size a and speed v [1,2,51], additionally tuned by the level of motility noise. The relative importance of SC increases with increasing motility noise, as reduced directional persistence negatively impacts TC.

It could have seemed tempting to use the ratio of signal-to-noise ratios SNR^{SC} and SNR^{TC} as a proxy for the relative importance of SC versus TC. However, this ratio depends on the choice of an effective measurement time, which can depend on model parameters in nontrivial ways [37–39]. Our Eq. (3) can thus be interpreted as an empirical power law for the effective measurement time.

We tested two prototypical decision rules, which represent two extremes of the fundamental exploitation-exploration trade-off: maximum likelihood and infotaxis. Both strategies exhibit similar performances, underscoring the generality of our results. While ML confines agents to the proximity of the target, resulting in a slight overall advantage, infotaxis initially performs better, as the persistent motion of agents right after their start increases information gain from TC. A mixed strategy, which balances exploitation and exploration, may thus optimize performance. Importantly, both strategies yield similar exponents for the empirical power law on the relative importance of TC versus SC (Table S2 in

the SM [40]). Similar exponents are also found if a different, exponential concentration field is used (Fig. S6 in the SM [40]).

The ideal chemotactic agent introduced here unifies previous theories of either pointlike chemotactic agents [20,21,25,27,31,32] (only TC) or extended but mostly stationary agents [16,17,38,55,56] (only SC). The increased usefulness of SC for larger agents was recently demonstrated in chemotactic agents equipped with small neuronal networks with SC and TC input trained with deep reinforcement learning [57]. An early computational work that addressed the importance of SC versus TC in a one-dimensional model (neglecting motility noise and assuming specific signaling circuits) identified the ratio between cell size and speed already as a key discriminator for the relative importance of SC [51], in line with the heuristic rule used in [2] and in agreement with our more general result.

Our analysis thus provides a theoretical underpinning for the previous heuristic notion on the evolutionary choice of different chemotaxis strategies in different cell types [1–3], which could be summarized as small and fast cells use TC, while large and slow (and less persistent) cells use SC. The power law derived here for a minimal model provides a robust predictor for this choice of chemotaxis strategy in single-celled organisms (see Fig. 4) despite the fact that biological cells have limited information processing capabilities and often need to navigate dynamic gradients [26,28,58,59]. While the optimal weighting of TC and SC could be different for chemotactic agents with limited information processing capabilities, our analysis for ideal agents indicates noise regimes, where SC or TC would provide little additional information, in semiquantitative agreement with data for biological cells. Moreover, the run-and-tumble motion of the bacterium *E. coli* shares features with the behavior of infotaxis agents in the limit of low motility noise, which comprises a straight run followed by a turn, which would be repeated if there were

an information reset after each turn. Biased random walks as observed for amoeboid cells in shallow gradients [6] emerge naturally in our minimal model.

Bayesian chemotaxis requires agents to have a model of typical search environments yet should be robust with respect to deviations between internal model and reality [38,60]. Supplemental simulations show that chemotactic agents still exhibit similar performance even if the assumed sensing-noise parameter or rotational diffusion coefficient used in their update step differs from the true value used to generate the input signal and simulate their motion (Figs. S7 and S8 in the SM [40]) or if concentration fields are distorted by shear or drift (Figs. S9 and S10). For biological cells, concentration fields may vastly differ for different cells and habitats [26,58], making it difficult to draw general conclusions. We thus resorted to an idealized yet prototypical case of a static concentration field shaped by a single source, which allows us to compare different chemotaxis strategies in a single model. In biological cells, knowledge about the environment (including characteristic dynamic changes [8,21,29,30,37,58,61]) is likely hard-wired in biochemical signaling networks and learned through evolutionary adaptation. Future work should address the impact of different gradient geometries and the timescale on which dynamic concentration fields change, yet this is beyond the scope of the present work.

Finally, there exists extended literature on odor tracking using sequential Bayesian updating, formulated as partially observable Markov decision processes [29–33,62]. This literature uses an equivalent terminology, which we briefly review in the SM [40]. Due to the lack of computationally efficient algorithms, heuristics were proposed to find near-optimal policies [25,32,33,63], of which infotaxis turned out to be surprisingly reliable, efficient, and safe [31]. Other algorithms performed slightly better in specific scenarios, but usually only with a 10% decrease in mean first-passage time to find a target and at the expense of reduced robustness [31,32]. This motivates our use of infotaxis as one of two decision rules tested.

In conclusion, an information-theoretical characterization of optimal chemotaxis as studied here for an ideal chemotactic agent, which weights gradient sensing in space and time, provides a baseline scenario to discuss the evolutionary choice of distinct gradient-sensing strategies under the pressure of sensing and motility noise.

The simulation data and PYTHON code for efficient simulation of the Bayesian chemotaxis investigated here are available in Ref. [64]. The data on speed and size of chemotactic cells analyzed in Fig. 4 are available as Supplemental Data of [2].

ACKNOWLEDGMENTS

J.R., M.N., and B.M.F. were supported by the German National Science Foundation (DFG) (Grant No. 391963627), the Center for Advancing Electronics Dresden (cfaed), and the Excellence Initiative by the German Federal and State Governments (Clusters of Excellence cfaed Grant No. EXC-1056 and Physics of Life Grant No. EXC-2068-390729961). B.M.F. was additionally supported by the DFG through a

Heisenberg grant (No. 421143374). We thank Andrea Aiconi for stimulating discussions. We thank Camillo Oeser and Arthur Willert for help with experiments, as well as the Center for Information Services at TU Dresden for granting use of their High Performance Computing facilities.

APPENDIX: ANALYTICAL THEORY

We review a minimal model of an ideal chemotactic agent subject to tunable sensing and motility noise previously developed in our group [34] and adapted for efficient simulations here. We first recall the mathematical theory from Ref. [34]. Equations (A2)–(A4) below are directly based on results derived there, though rewritten in more compact form that highlights information gain from SC and TC.

Following Ref. [34], we consider a disk-shaped agent of radius a and center position $\mathbf{x}_0(t)$, which searches for a hidden target at unknown position $\mathbf{x}^* = \mathbf{x}_0 + \mathbf{x}$ in the plane. The agent can detect signaling molecules diffusing from the target at each point $\mathbf{x}_e = \mathbf{x}_0 + a\mathbf{e}$ of its circumference at a rate density $\lambda c(\mathbf{x}_e)/2\pi a$ proportional to the local concentration $c(\mathbf{x}_e)$, where $c(\mathbf{x}) \sim 1/|\mathbf{x}|$ denotes the steady-state profile established by diffusion from a spherical source. We introduce a vector-valued chemotactic signal [38]

$$\mathbf{s}(t) = \sum_j \mathbf{e}_j \delta(t - t_j), \quad (\text{A1})$$

which records binding events occurring at time t_j at position $\mathbf{x}_0 + a\mathbf{e}_j$ on the agent's circumference, modeled as an inhomogeneous Poisson process [see the SM [40] for details and Fig. 1(b) for visualization]. The absolute value $s(t) = |\mathbf{s}(t)| = \sum \delta(t - t_j)$ is simply the train of binding events, ignoring their point of detection, as considered in [25]. If the target is assumed to be located at relative position \mathbf{x} , the conditional expectation value $\mathbb{E}(\mathbf{s}|\mathbf{x}) = \lambda a \nabla c/2$ of the vector signal $\mathbf{s}(t)$ encodes the local concentration gradient, while $J = \mathbb{E}(s|\mathbf{x})$ equals the rate of molecular binding events. This rate is proportional to the mean concentration along the circumference of the agent, $J \approx \lambda [c(\mathbf{x}_0) + (a^2/4)\nabla^2 c(\mathbf{x}_0)]$ [34].

The agent moves inside the concentration field with constant speed $v = |\mathbf{v}|$, subject to rotational diffusion with effective rotational diffusion coefficient D_{rot} , providing a minimal model of motility noise [38]. This dynamics extends the popular model of an active Brownian particle (ABP) [65], as our agent will continuously decide on its direction of motion based on the directional chemosensory input it receives.

We are interested in the information-theoretic limits of chemotaxis and therefore assume unlimited information processing capabilities of the agent, which can store and update a likelihood map $p(\mathbf{x}, t)$ of relative target position $\mathbf{x} = \mathbf{x}^* - \mathbf{x}_0$. The choice of an egocentric map, in which the moving agent is always at the center (with coordinate axes aligned to a comoving material frame of the agent), is mathematically convenient. We assume that the agent has implicit knowledge of stereotypic concentration fields and hence knows the conditional rate $J(\mathbf{x}_0|\mathbf{x}^*)$ and concentration gradient $\nabla_{\mathbf{x}_0} c(\mathbf{x}_0|\mathbf{x}^*)$, provided the target were at $\mathbf{x}^* = \mathbf{x}_0 + \mathbf{x}$. Here ∇c points towards the target.

Bayes' rule rationalizes how to update previous beliefs in light of new information. In a time-continuous formulation,

the time evolution of a likelihood map $p(\mathbf{x}, t)$ of relative target position reads

$$\begin{aligned} \frac{\partial}{\partial t} p(\mathbf{x}, t) = & \underbrace{[s - \mathbb{E}(s|s > 0)] \cdot \left(\frac{a\nabla c}{c} - \frac{\langle a\nabla c \rangle}{\langle c \rangle} \right) \frac{Jp}{\langle J \rangle}}_{\text{SC}} \\ & + \underbrace{(s - \mathbb{E}s) \left(\frac{J}{\langle J \rangle} - 1 \right) p}_{\text{TC}} + \underbrace{D_{\text{rot}} \frac{\partial^2 p}{\partial \varphi^2}}_{\text{motility noise}} \\ & + \underbrace{\mathbf{v} \cdot \nabla p}_{\text{coadvection}} + O(a^2), \end{aligned} \quad (\text{A2})$$

which follows from Ref. [34] after linearization by moment closure (see the SM [40] for details). This approximation is key for efficient numerical simulations. Different from Ref. [34] (and different from the usual Bayesian update scheme), we can now integrate the dynamics using substantially longer time steps that include multiple binding events. We confirmed in initial simulations that the full nonlinear scheme and our linearization gave essentially identical results. The expectation values $\mathbb{E}s$ and $\mathbb{E}(s|s > 0)$ denote measurements expected by the agent given its current likelihood map $p(\mathbf{x}, t)$, while $\langle \cdot \rangle$ averages over \mathbf{x} , again using $p(\mathbf{x}, t)$. Thus, $\mathbb{E}s = \langle \mathbb{E}(s|\mathbf{x}) \rangle$. Each summand on the right-hand side of Eq. (A2) has a straightforward physical interpretation. The third summand describes loss of information due to motility noise characterized as rotational diffusion, where φ denotes the polar angle of \mathbf{x} . The last summand describes the motion-induced shift of the egocentric map, in which the relative position of the target changes as $\dot{\mathbf{x}} = -\mathbf{v}$ when the agent moves with velocity \mathbf{v} . The TC term describes the update of target position based on the detection of signaling molecules, yet without reference to their position of detection on the circumference of the agent, thus generalizing TC. This term is equivalent to an analytical theory developed previously in Ref. [27] for the pointlike agents introduced in Ref. [25] and has a simple geometric interpretation: Whenever binding events are recorded at a rate higher than the expected detection rate (i.e., $s > \langle J \rangle$), the likelihood $p(\mathbf{x})$ is increased for all target positions \mathbf{x} , for which the local detection rate is higher than this mean rate [$J(\mathbf{x}) > \langle J \rangle$] but decreased for all other positions. For $s < \langle J \rangle$, this update has the opposite sign. In particular, even the absence of a binding event provides information to the agent, namely, that the target might be further away than expected [66].

The SC term is novel and describes the update due to spatial comparison of concentration differences across the diameter of the agent. This term is a scalar product of an innovation vector, formed by the difference of the vector-valued concentration measurement $\mathbf{s}(t)$ and its conditional

expectation value $\mathbb{E}(\mathbf{s}|s > 0) = \mathbb{E}\mathbf{s}s/\langle J \rangle$ if a binding event has happened, and the local concentration gradient, likewise corrected by a suitable expectation baseline. If no binding event is detected, the innovation vector is zero, reflecting the fact that it is impossible to record the position of a binding event without noticing that there has been a binding event in the first place.

Expected change in information. From the current prior $p(\mathbf{x}, t)$, the agent can infer the likelihood to detect a signaling molecule at a particular position and thus forecast how the negative Shannon entropy $I = \int d\mathbf{x} p(\mathbf{x}) \ln p(\mathbf{x})$ is expected to change in the infinitesimal time interval $[t, t + dt]$ ahead (see [34] and the SM [40] for details):

$$\begin{aligned} \mathbb{E} \frac{d}{dt} I = & \frac{1}{4} \underbrace{\left\langle J \left| \frac{a\nabla c}{c} - \frac{\langle a\nabla c \rangle}{\langle c \rangle} \right|^2 \right\rangle}_{\text{SC}} + \underbrace{\left\langle J \ln \left(\frac{J}{\langle J \rangle} \right) \right\rangle}_{\text{TC}} \\ & + \underbrace{D_{\text{rot}} \left\langle \frac{\partial^2}{\partial \varphi^2} \ln p \right\rangle}_{\text{motility noise}} + O(a^3). \end{aligned} \quad (\text{A3})$$

The SC term characterizes information gain due to spatial comparison and is always non-negative. If multiplied by a characteristic sensing time, this term generalizes the signal-to-noise ratio SNR^{SC} of spatial comparison [see Eq. (1)] by accounting for the expected gradient baseline $\langle \nabla c \rangle$. The TC term characterizes information gain due to temporal comparison; it is always greater than or equal to zero because it is proportional to the Kullback-Leibler divergence between the likelihood maps p and $pJ/\langle J \rangle$ before and after a binding event, respectively. The last summand characterizes information loss due to motility noise; this Fisher information is always less than or equal to zero by Bruijn's inequality [67].

Active motility with velocity \mathbf{v} affects the expected change of information only to second order in the time step, which can be expressed in terms of the time derivative of the expected change in information

$$\begin{aligned} \frac{d}{dt} \left(\mathbb{E} \frac{d}{dt} I \right) = & C + \underbrace{\left\langle \nabla \left(\frac{J}{4} \left| \frac{a\nabla c}{c} - \frac{\langle a\nabla c \rangle}{\langle c \rangle} \right|^2 \right) \right\rangle}_{\text{SC}} \cdot \mathbf{v} \\ & + \underbrace{\left\langle \ln \left(\frac{J}{\langle J \rangle} \right) \nabla J \right\rangle}_{\text{TC}} \cdot \mathbf{v} + O(a^3), \end{aligned} \quad (\text{A4})$$

where C combines terms independent of \mathbf{v} . Equation (A4) reformulates a result in Ref. [34] in more compact form (see the SM [40] for details). The first term characterizes information gain due to SC, whereas the second term characterizes information gain due to concentration sensing akin to TC.

- [1] D. B. Dusenbery, Spatial sensing of stimulus gradients can be superior to temporal sensing for free-swimming bacteria, *Biophys. J.* **74**, 2272 (1998).
 [2] K. Y. Wan and G. Jékely, Origins of eukaryotic excitability, *Philos. Trans. R. Soc. London B* **376**, 20190758 (2021).

- [3] L. Alvarez, B. M. Friedrich, G. Gompper, and U. B. Kaupp, The computational sperm cell, *Trends Cell Biol.* **24**, 198 (2014).
 [4] S. H. Zigmond, Mechanisms of sensing chemical gradients by polymorphonuclear leukocytes, *Nature (London)* **249**, 450 (1974).

- [5] C. A. Parent and P. N. Devreotes, A cell's sense of direction, *Science* **284**, 765 (1999).
- [6] P. J. Van Haastert and M. Postma, Biased random walk by stochastic fluctuations of chemoattractant-receptor interactions at the lower limit of detection, *Biophys. J.* **93**, 1787 (2007).
- [7] G. Amselem, M. Theves, A. Bae, C. Beta, and E. Bodenschatz, Control parameter description of eukaryotic chemotaxis, *Phys. Rev. Lett.* **109**, 108103 (2012).
- [8] A. Nakajima, S. Ishihara, D. Imoto, and S. Sawai, Rectified directional sensing in long-range cell migration, *Nat. Commun.* **5**, 5367 (2014).
- [9] H. C. Berg and D. A. Brown, Chemotaxis in *Escherichia coli* analysed by three-dimensional tracking, *Nature (London)* **239**, 500 (1972).
- [10] R. M. Macnab and D. E. Koshland, The gradient-sensing mechanism in bacterial chemotaxis, *Proc. Natl. Acad. Sci. USA* **69**, 2509 (1972).
- [11] J. E. Segall, S. M. Block, and H. C. Berg, Temporal comparisons in bacterial chemotaxis, *Proc. Natl. Acad. Sci. USA* **83**, 8987 (1986).
- [12] D. R. Brumley, F. Carrara, A. M. Hein, Y. Yawata, S. A. Levin, and R. Stocker, Bacteria push the limits of chemotactic precision to navigate dynamic chemical gradients, *Proc. Natl. Acad. Sci. USA* **116**, 10792 (2019).
- [13] H. H. Mattingly, K. Kamino, B. B. Machta, and T. Emonet, *Escherichia coli* chemotaxis is information limited, *Nat. Phys.* **17**, 1426 (2021).
- [14] J. F. Jikeli, L. Alvarez, B. M. Friedrich, L. G. Wilson, R. Pascal, R. Colin, M. Pichlo, A. Rennhack, C. Brenker, and U. B. Kaupp, Sperm navigation along helical paths in 3D chemoattractant landscapes, *Nat. Commun.* **6**, 7985 (2015).
- [15] H. C. Berg and E. M. Purcell, Physics of chemoreception., *Biophys. J.* **20**, 193 (1977).
- [16] R. G. Endres and N. S. Wingreen, Accuracy of direct gradient sensing by single cells, *Proc. Natl. Acad. Sci. USA* **105**, 15749 (2008).
- [17] B. Hu, W. Chen, W.-J. Rappel, and H. Levine, Physical limits on cellular sensing of spatial gradients, *Phys. Rev. Lett.* **105**, 048104 (2010).
- [18] W. Bialek and S. Setayeshgar, Physical limits to biochemical signaling, *Proc. Natl. Acad. Sci. USA* **102**, 10040 (2005).
- [19] K. Kaizu, W. De Ronde, J. Paijmans, K. Takahashi, F. Tostevin, and P. R. ten Wolde, The Berg-Purcell limit revisited, *Biophys. J.* **106**, 976 (2014).
- [20] T. Mora and N. S. Wingreen, Limits of sensing temporal concentration changes by single cells, *Phys. Rev. Lett.* **104**, 248101 (2010).
- [21] A. M. Hein, D. R. Brumley, F. Carrara, R. Stocker, and S. A. Levin, Physical limits on bacterial navigation in dynamic environments, *J. R. Soc. Interface* **13**, 20150844 (2016).
- [22] D. Fuller, W. Chen, M. Adler, A. Groisman, H. Levine, W.-J. Rappel, and W. F. Loomis, External and internal constraints on eukaryotic chemotaxis, *Proc. Natl. Acad. Sci. USA* **107**, 9656 (2010).
- [23] K. L. Thornton, J. K. Butler, S. J. Davis, B. K. Baxter, and L. G. Wilson, Haloarchaea swim slowly for optimal chemotactic efficiency in low nutrient environments, *Nat. Commun.* **11**, 4453 (2020).
- [24] K. Nakamura and T. J. Kobayashi, Optimal sensing and control of run-and-tumble chemotaxis, *Phys. Rev. Res.* **4**, 013120 (2022).
- [25] M. Vergassola, E. Villermaux, and B. Shraiman, 'Infotaxis' as a strategy for searching without gradients, *Nature (London)* **445**, 406 (2007).
- [26] A. Celani and M. Vergassola, Bacterial strategies for chemotaxis response, *Proc. Natl. Acad. Sci. USA* **107**, 1391 (2010).
- [27] C. Barbieri, S. Cocco, and R. Monasson, On the trajectories and performance of infotaxis, an information-based greedy search algorithm, *Europhys. Lett.* **94**, 20005 (2011).
- [28] B. Hartl, M. Hübl, G. Kahl, and A. Zöttl, Microswimmers learning chemotaxis with genetic algorithms, *Proc. Natl. Acad. Sci. USA* **118**, e2019683118 (2021).
- [29] N. Rigolli, N. Magnoli, L. Rosasco, and A. Seminara, Learning to predict target location with turbulent odor plumes, *eLife* **11**, e72196 (2022).
- [30] G. Reddy, V. N. Murthy, and M. Vergassola, Olfactory sensing and navigation in turbulent environments, *Annu. Rev. Condens. Matter Phys.* **13**, 191 (2022).
- [31] A. Loisy and C. Eloy, Searching for a source without gradients: how good is infotaxis and how to beat it, *Proc. R. Soc. A* **478**, 20220118 (2022).
- [32] A. Loisy and R. A. Heinonen, Deep reinforcement learning for the olfactory search POMDP: a quantitative benchmark, *Eur. Phys. J. E* **46**, 17 (2023).
- [33] A. R. Cassandra, L. P. Kaelbling, and J. A. Kurien, in *Proceedings of the IEEE/RSJ International Conference on Intelligent Robots and Systems, Osaka, 1996* (IEEE, Piscataway, NJ, 1996), Vol. 2, pp. 963–972.
- [34] A. Auconi, M. Novak, and B. M. Friedrich, Gradient sensing in Bayesian chemotaxis, *Europhys. Lett.* **138**, 12001 (2022).
- [35] A. Bain and D. Crisan, *Fundamentals of Stochastic Filtering* (Springer, Berlin, 2009).
- [36] S. P. Strong, B. Freedman, W. Bialek, and R. Koberle, Adaptation and optimal chemotactic strategy for *E. coli*, *Phys. Rev. E* **57**, 4604 (1998).
- [37] T. Mora and I. Nemenman, Physical limit to concentration sensing in a changing environment, *Phys. Rev. Lett.* **123**, 198101 (2019).
- [38] M. Novak and B. M. Friedrich, Bayesian gradient sensing in the presence of rotational diffusion, *New J. Phys.* **23**, 043026 (2021).
- [39] R. O. P. Ramakrishnan and B. M. Friedrich, Learning run-and-tumble chemotaxis with support vector machines, *Europhys. Lett.* **142**, 47001 (2023).
- [40] See Supplemental Material at <http://link.aps.org/supplemental/10.1103/PRXLife.2.023012> for additional details on numerical methods, analytic theory, and experiments.
- [41] J. A. Kromer, A. Auconi, and B. M. Friedrich, Composite search of active particles in three-dimensional space based on non-directional cues, *ChemNanoMat* **7**, 1057 (2021).
- [42] B. M. Friedrich, Search along persistent random walks, *Phys. Biol.* **5**, 026007 (2008).
- [43] K. J. Åström, Optimal control of Markov processes with incomplete state information, *J. Math. Anal. Appl.* **10**, 174 (1965).
- [44] R. D. Smallwood and E. J. Sondik, The optimal control of partially observable Markov processes over a finite horizon, *Oper. Res.* **21**, 1071 (1973).

- [45] C. Baier and J.-P. Katoen, *Principles of Model Checking* (MIT Press, Cambridge, 2008).
- [46] P. Massart, The tight constant in the Dvoretzky-Kiefer-Wolfowitz inequality, *Ann. Probab.* **18**, 1269 (1990).
- [47] J. H. R. Wheeler, K. R. Foster, and W. M. Durham, Individual bacterial cells can use spatial sensing of chemical gradients to direct chemotaxis on surfaces, *Nat. Microbiol.* (to be published), [bioRxiv:10.1101/2024.02.13.580113](https://doi.org/10.1101/2024.02.13.580113).
- [48] R. Thar and M. Kühl, Bacteria are not too small for spatial sensing of chemical gradients: An experimental evidence, *Proc. Natl. Acad. Sci. USA* **100**, 5748 (2003).
- [49] A. Einstein, Zur Theorie der Brownschen Bewegung [AdP 19, 371 (1906)], *Ann. Phys. (Leipzig)* **517**, 248 (1906/2005).
- [50] H. Crenshaw, A new look at locomotion in microorganisms: rotating and translating, *Am. Zool.* **36**, 608 (1996).
- [51] R. Z. Tan and K.-H. Chiam, A computational model for how cells choose temporal or spatial sensing during chemotaxis, *PLoS Comput. Biol.* **14**, e1005966 (2018).
- [52] E. M. Moraud and D. Martinez, Effectiveness and robustness of robot infotaxis for searching in dilute conditions, *Front. Neurobot.* **4**, 1 (2010).
- [53] J.-B. Masson, Olfactory searches with limited space perception, *Proc. Natl. Acad. Sci. USA* **110**, 11261 (2013).
- [54] N. Voges, A. Chaffiol, P. Lucas, and D. Martinez, Reactive searching and infotaxis in odor source localization, *PLoS Comput. Biol.* **10**, e1003861 (2014).
- [55] U. Dobramysl and D. Holcman, Triangulation sensing to determine the gradient source from diffusing particles to small cell receptors, *Phys. Rev. Lett.* **125**, 148102 (2020).
- [56] K. Nakamura and T. J. Kobayashi, Gradient sensing limit of a cell when controlling the elongating direction, [arXiv:2405.04810](https://arxiv.org/abs/2405.04810).
- [57] A. Alonso and J. B. Kirkegaard, Learning optimal integration of spatial and temporal information in noisy chemotaxis, [arXiv:2310.10531](https://arxiv.org/abs/2310.10531) [PNAS Nexus (to be published)].
- [58] R. Stocker, Marine microbes see a sea of gradients, *Science* **338**, 628 (2012).
- [59] S. Lange and B. M. Friedrich, Sperm chemotaxis in marine species is optimal at physiological flow rates according to theory of filament surfing, *PLoS Comput. Biol.* **17**, e1008826 (2021).
- [60] J. D. Rodríguez, D. Gómez-Ullate, and C. Mejía-Monasterio, On the performance of blind-infotaxis under inaccurate modeling of the environment, *Eur. Phys. J.: Spec. Top.* **226**, 2407 (2017).
- [61] A. Celani, E. Villermaux, and M. Vergassola, Odor landscapes in turbulent environments, *Phys. Rev. X* **4**, 041015 (2014).
- [62] K. V. B. Verano, E. Panizon, and A. Celani, Olfactory search with finite-state controllers, *Proc. Natl. Acad. Sci. USA* **120**, e2304230120 (2023).
- [63] J. Kromer, S. Märcker, S. Lange, C. Baier, and B. M. Friedrich, Decision making improves sperm chemotaxis in the presence of noise, *PLoS Comput. Biol.* **14**, e1006109 (2018).
- [64] <https://zenodo.org/records/11352807>
- [65] P. Romanczuk, M. Bär, W. Ebeling, B. Lindner, and L. Schimansky-Geier, Active brownian particles, *Eur. Phys. J.: Spec. Top.* **202**, 1 (2012).
- [66] A. M. Hein and S. A. McKinley, Sensing and decision-making in random search, *Proc. Natl. Acad. Sci. USA* **109**, 12070 (2012).
- [67] A. Dembo, T. M. Cover, and J. A. Thomas, Information theoretic inequalities, *IEEE Trans. Inf. Theory* **37**, 1501 (1991).

Correction: The fourth sentence of the last paragraph of the Introduction has been modified.